

Constraints on Single-Field Inflation from the BOSS Galaxy Survey

Giovanni Cabass,^{1,*} Mikhail M. Ivanov,^{1,†} Oliver H. E. Philcox,^{2,1} Marko Simonović,³ and Matias Zaldarriaga¹

¹*School of Natural Sciences, Institute for Advanced Study, 1 Einstein Drive, Princeton, NJ 08540, USA*

²*Department of Astrophysical Sciences, Princeton University, Princeton, NJ 08540, USA*

³*Theoretical Physics Department, CERN, 1 Esplanade des Particules, Geneva 23, CH-1211, Switzerland*

Non-local primordial non-Gaussianity (NLPNG) is a smoking gun of interactions in single-field inflationary models, and can be written as a combination of the equilateral and orthogonal templates. We present the first constraints on these from the redshift-space galaxy power spectra and bispectra of the Baryon Oscillation Spectroscopic Survey (BOSS) data. These are the first such measurements independent of the cosmic microwave background fluctuations. We perform a consistent analysis that includes all necessary nonlinear corrections generated by NLPNG, and vary all relevant cosmological and nuisance parameters in a global fit to the data. Our conservative analysis yields joint limits on the amplitudes of the equilateral and orthogonal shapes, $f_{\text{NL}}^{\text{equil}} = 940 \pm 600$, $f_{\text{NL}}^{\text{ortho}} = -170 \pm 170$ (both at 68% CL). These can be used to derive constraints on coefficients of the effective single-field inflationary Lagrangian; in particular, we find that the sound speed of inflaton fluctuations has the bound $c_s \geq 0.013$ at 95% CL. Fixing the quadratic galaxy bias and cosmological parameters, the constraints can be tightened to $f_{\text{NL}}^{\text{equil}} = 260 \pm 300$, $f_{\text{NL}}^{\text{ortho}} = -23 \pm 120$ (68% CL).

Introduction — Cosmology is the interface between particle physics and general relativity. Nothing exemplifies this more than inflation – a primordial accelerated expansion of the Universe that may have happened at energy scales as high as 10^{14} GeV. Inflation naturally generates quantum fluctuations that provide the seeds for the formation and clustering of matter and galaxies. Thus, observations of the large-scale structure of our Universe allow us to probe physics at these extremely high energies, inaccessible to present-day particle accelerators.

There are three main questions about inflation one may ask: What is its energy scale? How many degrees of freedom generated density fluctuations? How fast did these degrees of freedom propagate? While significant efforts have been devoted to answering the first question, by constraining the amplitude of primordial gravitational waves, the latter two require a probe of deviations of the initial density fluctuations from a Gaussian distribution, known as primordial non-Gaussianity (PNG).

The simplest observable encoding PNG is the bispectrum, B_ζ , of the primordial metric curvature perturbation ζ . Due to translational and rotational invariance, B_ζ is a function of the moduli of three momenta, $\mathbf{k}_1, \mathbf{k}_2, \mathbf{k}_3$, which form a closed triangle. A bispectrum peaking at squeezed triangles, $k_1 \ll k_2 \approx k_3$, is a generic signa-

ture of particle interactions in multi-field inflation [1–9],¹ i.e. where more than one degree of freedom is light during inflation. This type of PNG is called “local”. In contrast, a bispectrum peaking at equilateral ($k_1 \approx k_2 \approx k_3$) or flattened ($k_1 \approx k_2 \approx k_3/2$) triangles is a peculiar feature of interactions in single-field inflation [12–19], which has only one degree of freedom (inflaton). This kind of “non-local” primordial non-Gaussianity (NLPNG) can be represented as a linear combination of two basis shapes, equilateral and orthogonal [19], with amplitudes $f_{\text{NL}}^{\text{equil}}$ and $f_{\text{NL}}^{\text{ortho}}$ respectively.

Symmetries of inflation also dictate a relationship between the inflaton speed of sound and the strength of nonlinear interactions that generate NLPNG [17]. In particular, there is a theorem stating that PNG can be large if and only if the sound speed is small [20, 21]. This allows one to constrain the propagation speed of the inflaton from the observed level of NLPNG.

Up to now, the only source of information on NLPNG has been the cosmic microwave background (CMB) temperature and polarization data [11, 22]. In particular, *Planck* 2018 data yield $f_{\text{NL}}^{\text{equil}} = -26 \pm 47$, $f_{\text{NL}}^{\text{ortho}} = -38 \pm 24$ (both at 68% CL) [11]. In theory, one can obtain better constraints with upcoming galaxy surveys,

* gcabass@ias.edu

† Einstein Fellow; ivanov@ias.edu

¹ These shapes also appear in ekpyrotic alternatives to inflation (see Ref. [10] for a review), but they typically produce strong PNG incompatible with data [11].

which will collect orders of magnitude more cosmological information as counted in number of accessible Fourier modes. However, the analysis of this data is also more intricate because PNG in the galaxy distribution is a weak effect on top of an intrinsic, late-time non-Gaussian signal generated by nonlinear clustering of matter. Thus, late-time nonlinearities act as background noise, which must be accurately modeled if we are to measure PNG from large-scale structure data.

There have been significant efforts to probe *local* PNG from galaxy surveys, exploiting the scale-dependent bias that enhances the observed power spectrum on very large scales [23–25]. This enhancement originates from a particular form of the squeezed limit of the local shape. NLPNG is different as the relevant shapes are suppressed in the squeezed limit and hence do not produce significant scale-dependent bias. Thus, this type of PNG requires a dedicated study. Indeed, the leading effect of NLPNG on galaxy clustering is a specific shape dependence in the galaxy bispectrum, which also modulates power spectra through loop corrections. These effects can be constrained by a systematic analysis based on the consistently-modeled power spectrum and bispectrum data. In this *Letter*, we present the first such analysis of the publicly available state of the art redshift clustering data from the Baryon Oscillation Spectroscopic Survey (BOSS).

A rigorous analysis of the galaxy bispectrum has been a long-time challenge. Even ignoring PNG, the complete theoretical model including all necessary effects relevant for the actual data has been developed only recently [26, 27] (see also [28–40]). On the data side, a major improvement has come from the estimators that remove effects of the survey window function [41, 42]. These efforts now allow us to obtain the first CMB-independent limits on NLPNG from galaxy redshift surveys.

PNG in single-field inflation — A general single-field Lagrangian for the inflaton perturbation π with leading interactions up to cubic order is given by [17, 19]

$$S_{\text{EFT}} = \int d^4x \sqrt{-g} \left[-\frac{M_P^2 \dot{H}}{c_s^2} \left(\dot{\pi}^2 - c_s^2 \frac{(\nabla \pi)^2}{a^2} \right) + \frac{M_P^2 \dot{H}}{c_s^2} (1 - c_s^2) \left(\frac{\dot{\pi}(\nabla \pi)^2}{a^2} - \left(1 + \frac{2}{3} \tilde{c}_3 \frac{c_s^2}{\dot{c}_3^2} \right) \dot{\pi}^3 \right) \right]. \quad (1)$$

π is related to the metric curvature perturbation via $\zeta = -H\pi$, with H being the Hubble parameter during

inflation. The two inflaton interactions are parametrized by the sound speed c_s and a dimensionless Wilson coefficient \tilde{c}_3 . It is customary to represent PNG produced by these interactions as a linear combination of the orthogonal and equilateral templates. To that end, we define

$$B_\zeta(k_1, k_2, k_3) = \frac{18}{5} f_{\text{NL}} \Delta_\zeta^4 \frac{\mathcal{S}(k_1, k_2, k_3)}{k_1^2 k_2^2 k_3^2}. \quad (2)$$

Here, Δ_ζ^2 is the amplitude of the primordial power spectrum: $k^3 P_\zeta(k) = \Delta_\zeta^2 (k/k_*)^{n_s-1}$, where n_s is the spectral index. Analysis of *Planck* data finds $\Delta_\zeta^2 \approx 4.1 \times 10^{-8}$, $n_s \approx 0.96$ [43] for the pivot scale $k_* = 0.05 \text{ Mpc}^{-1}$. The equilateral and orthogonal templates are defined as [19, 44]²

$$\begin{aligned} \mathcal{S}_{\text{equil}}(k_1, k_2, k_3) &= \left(\frac{k_1}{k_2} + 5 \text{ perms.} \right) - \left(\frac{k_1^2}{k_2 k_3} + 2 \text{ perms.} \right) - 2, \\ \mathcal{S}_{\text{ortho}}(k_1, k_2, k_3) &= (1+p) \frac{\Delta}{e_3} - p \frac{\Gamma^3}{e_3^2}, \end{aligned} \quad (3)$$

where $p = 8.52587$, $\Delta = (k_T - 2k_1)(k_T - 2k_2)(k_T - 2k_3)$,

$$\begin{aligned} k_T &= k_1 + k_2 + k_3, & e_2 &= k_1 k_2 + k_2 k_3 + k_1 k_3, \\ e_3 &= k_1 k_2 k_3, & \Gamma &= \frac{2}{3} e_2 - \frac{1}{3} (k_1^2 + k_2^2 + k_3^2). \end{aligned} \quad (4)$$

The amplitudes $f_{\text{NL}}^{\text{equil}}$, $f_{\text{NL}}^{\text{ortho}}$ are related to the coefficients of the EFT Lagrangian via [19, 44]

$$\begin{aligned} \begin{pmatrix} f_{\text{NL}}^{\text{equil}} \\ f_{\text{NL}}^{\text{ortho}} \end{pmatrix} &= \begin{pmatrix} 1.04021 & 1.21041 \\ -0.0395140 & -0.175685 \end{pmatrix} \begin{pmatrix} f_{\text{NL}}^{\dot{\pi}(\nabla \pi)^2} \\ f_{\text{NL}}^{\dot{\pi}^3} \end{pmatrix}, \\ f_{\text{NL}}^{\dot{\pi}(\nabla \pi)^2} &= \frac{85}{324} (1 - c_s^{-2}), \\ f_{\text{NL}}^{\dot{\pi}^3} &= \frac{10}{243} (1 - c_s^{-2}) \left(\tilde{c}_3 + \frac{3}{2} c_s^2 \right). \end{aligned} \quad (5)$$

Large Scale Structure in the presence of NLPNG — Before considering NLPNG, we first discuss structure formation in a Universe with Gaussian initial conditions. We describe it in the framework of the effective field theory of large-scale structure (EFTofLSS), where one builds

² Note that we use the orthogonal template from Appendix B of [19], which has a physically correct suppression in the squeezed limit $k_1 \ll k_2 \approx k_3$, where it goes as $\mathcal{S}_{\text{ortho}} \propto k_1/k_3$. It can be contrasted with the commonly used approximate template that features an unphysical enhancement in that limit [11].

a perturbative expansion in terms of the linear matter overdensity field $\delta^{(1)}$ (see [33, 34, 45–48] and references therein). For Gaussian initial conditions, statistical properties of $\delta^{(1)}$ are fully determined by its power spectrum³ P_{11}

$$\langle \delta^{(1)}(\mathbf{k})\delta^{(1)}(\mathbf{k}') \rangle = (2\pi)^3 \delta_D^{(3)}(\mathbf{k}' + \mathbf{k}) P_{11}(k) . \quad (6)$$

We restrict our galaxy power spectrum analysis to the one-loop order in the EFTofLSS. In the absence of NLPNG, the nonlinear power spectrum takes the following schematic form

$$P_G \equiv P_{11} + P_{1\text{-loop}} + P_{\text{ctr}} + P_{\text{stoch}} , \quad (7)$$

where $P_{1\text{-loop}}$ is the nonlinear one-loop correction for Gaussian initial conditions, P_{ctr} is the counterterm that stems from the higher-derivative operators in the fluid equation and the bias expansion, while P_{stoch} captures galaxy stochasticity. Nonlinear clustering also generates a non-trivial “Gaussian” bispectrum B_G , which we consider here in the tree-level approximation.

PNG affects large-scale structure via three channels: initial conditions, loop corrections, and scale-dependent galaxy bias. First, PNG induces a bispectrum signal additional to the one coming from nonlinear mode coupling [49, 50],

$$\begin{aligned} \langle \delta^{(1)}\delta^{(1)}\delta^{(1)} \rangle &= f_{\text{NL}} B_{111}(k_1, k_2, k_3) (2\pi)^3 \delta_D^{(3)}(\mathbf{k}_{123}) , \\ f_{\text{NL}} B_{111}(k_1, k_2, k_3) &= \mathcal{T}(k_1)\mathcal{T}(k_2)\mathcal{T}(k_3)B_\zeta(k_1, k_2, k_3) , \end{aligned} \quad (8)$$

where $\mathbf{k}_{123} = \mathbf{k}_1 + \mathbf{k}_2 + \mathbf{k}_3$, and we introduced the transfer functions $\mathcal{T}(k) \equiv \delta^{(1)}(\mathbf{k})/\zeta(\mathbf{k}) = (P_{11}(k)/P_\zeta(k))^{1/2}$. The initial bispectrum (8) also leaks into the nonlinear galaxy power spectra through mode coupling, and induces the following non-Gaussian one-loop correction (which adds to P_G above)

$$\begin{aligned} f_{\text{NL}} P_{12}(\mathbf{k}) &= 2f_{\text{NL}} Z_1(\mathbf{k}) \\ &\times \int \frac{d^3 q}{(2\pi)^3} Z_2(\mathbf{q}, \mathbf{k} - \mathbf{q}) B_{111}(k, q, |\mathbf{k} - \mathbf{q}|) . \end{aligned} \quad (9)$$

Here $Z_{1,2}$ are linear and quadratic galaxy redshift-space kernels [51], $Z_1(\mathbf{k}) = b_1 + f(\hat{\mathbf{k}} \cdot \hat{\mathbf{z}})^2$ where f is the logarithmic growth factor, $\hat{\mathbf{z}}$ is the line-of-sight direction unit

vector, and $\hat{\mathbf{k}} \equiv \mathbf{k}/k$. The P_{12} terms are present for both galaxies and matter [52–54], and we will refer to them as “NG matter loops” in what follows.

Third, NLPNG modulates galaxy formation, which is captured on large scales by the scale-dependent galaxy bias [47, 55, 56],⁴

$$\delta_g = b_1 \delta + f_{\text{NL}} b_\zeta (k/k_{\text{NL}})^2 \zeta + \text{nonlinear} , \quad (10)$$

where δ and δ_g are overdensity fields of matter and galaxies respectively, b_1 is the usual linear bias, b_ζ is an order-one PNG linear bias coefficient, and $k_{\text{NL}} \approx 0.5 h\text{Mpc}^{-1}$ is the nonlinear scale⁵ at the relevant redshift $z \simeq 0.5$.

The relative size of various perturbative corrections can be estimated using the scaling universe approach [53, 57]. It is based on the observation that the linear power spectrum can be well approximated by a power-law $P_{11} \propto (k/k_{\text{NL}})^n k_{\text{NL}}^{-3}$ with $n \approx -1.7$ for quasi-linear wavenumbers $k \simeq 0.15 h\text{Mpc}^{-1}$. Assuming that there is a single nonlinear scale in the problem, the scaling universe estimates suggest that the leading non-Gaussian corrections are the PNG matter loops and the linear scale-dependent bias. The total dimensionless galaxy power spectrum $\Delta^2(k) \equiv k^3 P(k)/(2\pi^2)$ can be estimated as

$$\begin{aligned} \Delta^2(k) &= \underbrace{\left(\frac{k}{k_{\text{NL}}}\right)^{1.3}}_{\text{tree}} + \underbrace{\left(\frac{k}{k_{\text{NL}}}\right)^{2.6}}_{1\text{-loop}} + \underbrace{\left(\frac{k}{k_{\text{NL}}}\right)^{3.3}}_{\text{ctr}} + \underbrace{\left(\frac{k}{k_{\text{NL}}}\right)^3}_{\text{stoch}} \\ &+ \underbrace{f_{\text{NL}} \Delta_\zeta \left(\frac{k}{k_{\text{NL}}}\right)^{1.95}}_{\text{NG matter loops}} + \underbrace{f_{\text{NL}} b_\zeta \Delta_\zeta \left(\frac{k}{k_{\text{NL}}}\right)^{2.65}}_{\text{linear PNG bias}} . \end{aligned} \quad (11)$$

All higher order corrections, such as PNG terms $\mathcal{O}(f_{\text{NL}}^2)$, NG two-loop corrections, contributions generated by nonlinear bias operators like $\delta \nabla^2 \zeta$, and Gaussian two-loop corrections, are subleading for $f_{\text{NL}} \Delta_\zeta \lesssim 0.1$ and $k \lesssim 0.17 h\text{Mpc}^{-1}$ typical for our analysis, and hence can be neglected.⁶ This will be validated on the mock simulation data below. As for the bispectrum, we use the tree-level approximation so only the leading PNG bispectrum (8) is of importance [53].

⁴ Equilateral and orthogonal PNG produce identical scale-dependent biases that can be captured by a single free parameter.

⁵ Defined by $P_{11}(k_{\text{NL}}) k_{\text{NL}}^3 / (2\pi^2) = 1$.

⁶ For local-type PNG the situation is different: the PNG bias terms dominate on large scales.

³ We suppress the explicit time dependence for brevity.

All in all, our final model for the galaxy power spectra and bispectra in redshift space is given by

$$\begin{aligned} P(\mathbf{k}) &= P_G(\mathbf{k}) + f_{NL} \left(P_{12}(\mathbf{k}) + \frac{2b_\zeta Z_1(\mathbf{k})k^2}{k_{NL}^2} \frac{P_{11}(k)}{\mathcal{T}(k)} \right), \\ B(\mathbf{k}_1, \mathbf{k}_2, \mathbf{k}_3) &= B_G(\mathbf{k}_1, \mathbf{k}_2, \mathbf{k}_3) \\ &+ f_{NL} Z_1(\mathbf{k}_1) Z_1(\mathbf{k}_2) Z_1(\mathbf{k}_3) B_{111}(k_1, k_2, k_3), \end{aligned} \quad (12)$$

where P_G and B_G are the standard Gaussian power spectrum and bispectrum models [26, 58]. In practice, we compute the Legendre redshift-space multipoles P_ℓ ($\ell = 0, 2, 4$) of the galaxy power spectrum and use the angle-averaged (monopole) bispectrum. We also implement IR resummation in redshift space [59–64] (to account for long-wavelength displacement effects) and the Alcock-Paczynski effect [65] (to account for coordinate conversions [33]).

Our model has 14 nuisance parameters: 13 standard bias parameters and counterterms of Gaussian redshift-space power spectra and bispectra (present in previous analyses), plus the scale-dependent PNG bias b_ζ (10).

Data and Analysis — We use the twelfth data release (DR12) [66] of BOSS. The data is split into two redshift bins with effective means $z = 0.38, 0.61$, in each of the Northern and Southern galactic caps, resulting in four independent data chunks. The survey contains $\sim 1.2 \times 10^6$ galaxy positions with a total volume of $6(h^{-1}\text{Gpc})^3$. From each chunk, we use the power spectrum multipoles ($\ell = 0, 2, 4$) for $k \in [0.01, 0.17] h\text{Mpc}^{-1}$, the real-space power spectrum Q_0 for $k \in [0.17, 0.4] h\text{Mpc}^{-1}$ [67], the redshift-space bispectrum monopoles for triangle configurations within the range of $k_i \in [0.01, 0.08] h\text{Mpc}^{-1}$ (62 triangles), and the BAO parameters extracted from the post-reconstructed power spectrum data [68], as in [27]. The power spectra and bispectra are measured with the window-free estimators [41, 42]. The covariances for each data chunk are computed from a suite of 2048 MultiDark-Patchy mocks [69].

We perform the full-shape analysis of the redshift clustering data following the methodology of [27, 33, 34, 68]. We implement the complete theory model for the power spectra and bispectra of galaxies in redshift space in an extension of the CLASS-PT code [51]⁷ that includes

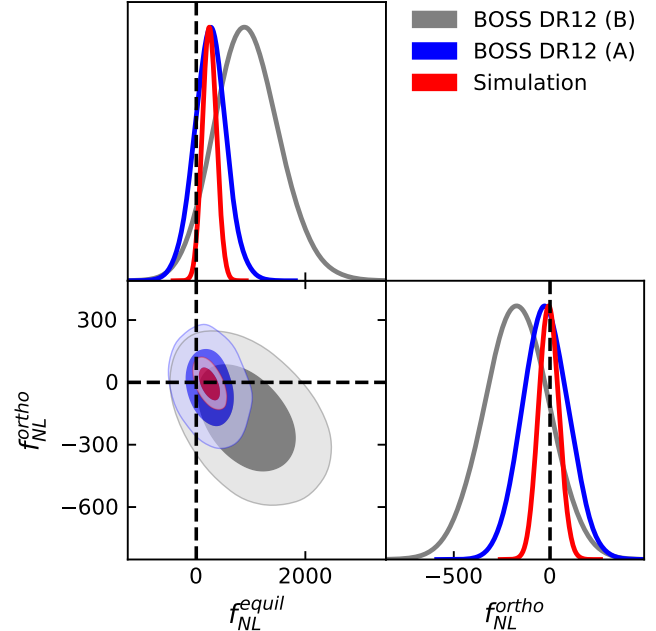


FIG. 1. Marginalized constraints on parameters $(f_{NL}^{equil}, f_{NL}^{ortho})$ from the BOSS data obtained in the conservative baseline analysis (BOSS DR12 (B), gray), and in the aggressive analysis (BOSS DR12 (A), blue). We also show results from the full Nseries simulation suite (red), whose volume is 40 times larger than BOSS. Dashed lines indicate $f_{NL}^{equil} = 0, f_{NL}^{ortho} = 0$.

all non-Gaussian corrections described above (computed using the FFTlog approach [70]). We consistently recompute the shape of these corrections as we scan over different cosmologies in a Markov Chain Monte Carlo (MCMC) analysis. Up to additional NG contributions, our analysis is identical to [27].

In our baseline analysis we fix the baryon density to the BBN measurement [71], the primordial power spectrum tilt to the Planck best-fit value [43], and the neutrino mass to the minimal value allowed by oscillation experiments $\sum m_\nu = 0.06$ eV. We vary the physical dark matter density ω_{cdm} , the reduced Hubble parameter h , the amplitude of the primordial scalar fluctuations $\ln(10^{10} A_s)$, and $(f_{NL}^{equil}, f_{NL}^{ortho})$ within flat infinitely wide priors. We use the same priors for nuisance parameters as [27]. We also marginalize over the linear PNG bias, $b_\zeta = 1.686 \cdot \frac{18}{5}(b_1 - 1)\tilde{b}_\zeta$ within a Gaussian prior

⁷ Code available at github.com/Michalychforever/CLASS-PT

PT, with custom MontePython likelihoods available at github.com/oliverphilcox/full_shape_likelihoods.

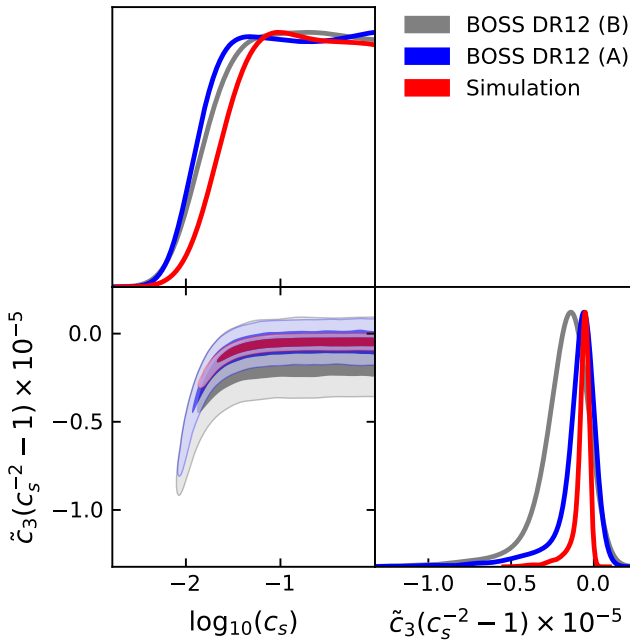


FIG. 2. Marginalized constraints on single-field inflation parameters (c_s , \tilde{c}_3) from the BOSS data in the baseline analysis (BOSS DR12 (B), gray), aggressive analysis (BOSS DR12 (A), blue), and from the full Nseries simulation suite (red).

$\tilde{b}_\zeta \sim \mathcal{N}(1, 5)$ motivated by the peak-background split model [72].

In addition, we perform a more aggressive analysis, whereupon cosmological parameters are set to the *Planck* 2018 priors. Moreover, instead of marginalization, we fix the quadratic galaxy biases to predictions of the standard dark matter halo relations [47]. These agree with simulations at the level required by the BOSS data [26, 36].

It is worth noting that our analysis is different from the CMB one [19], where f_{NL} is estimated directly from the temperature and polarization maps. In contrast, we do a global fit to the summary statistics, and vary f_{NL}^{equil} , f_{NL}^{ortho} along with all other cosmological and nuisance parameters in our MCMC chains, necessary due to the appearance of parameter-dependent late-time non-Gaussianity.

Results — First, we apply our pipeline to Nseries mock catalogs. These are based on high-resolution N-body simulations and were used by the BOSS collaboration for validation tests [66]. The cumulative volume of this simulation is $235 (h^{-1}\text{Gpc})^3$, which is ≈ 40 times larger than actual BOSS survey volume. The mocks were generated from purely Gaussian initial conditions, which we must recover with our pipeline as a consistency check. Indeed,

we find $f_{NL}^{\text{equil}} = 240^{+130}_{-130}$, $f_{NL}^{\text{ortho}} = -6^{+52}_{-54}$, which is consistent with $f_{NL}^{\text{equil}} = 0$ within 95% CL and $f_{NL}^{\text{ortho}} = 0$ within 68% CL. The shift in f_{NL}^{equil} , even if statistically insignificant, yields an estimate of the theoretical uncertainty, $\Delta f_{NL}^{\text{equil}} \lesssim 100$, which is less than 0.2σ of the BOSS 1d marginalized statistical error. This is consistent with estimates of higher order perturbative corrections that are omitted in our analysis. We have also found that the constraints are driven by the bispectrum: the power spectrum data alone gives $f_{NL}^{\text{equil}} = -640 \pm 1200$, $f_{NL}^{\text{ortho}} = 2400 \pm 1600$ (at 68% CL).

Having validated our method on the simulations, we move to the actual BOSS data. Our baseline MCMC analysis yields the following 1d marginalized estimates of equilateral and orthogonal f_{NL} values from the joint fit:

$$f_{NL}^{\text{equil}} = 940^{+570}_{-650}, \quad f_{NL}^{\text{ortho}} = -170^{+180}_{-170}, \quad (68\% \text{ CL}). \quad (13)$$

We do not find any evidence for NLPNG: the 95% CL limits read

$$-280 < f_{NL}^{\text{equil}} < 2190, \quad -520 < f_{NL}^{\text{ortho}} < 176. \quad (14)$$

The resulting posterior contours are shown in Fig. 1. The correlation coefficient between the equilateral and orthogonal shapes is -0.40 . The best measured principal component is

$$f_{NL}^{\text{ortho}} - 0.11f_{NL}^{\text{equil}} = -65 \pm 157.$$

Note that the correlation is dictated by degeneracy directions in the shape of the BOSS galaxy bispectrum. This can be contrasted with the *Planck* 2018 data that does not show any appreciable degeneracy between the two shapes, i.e. their correlation matches the intrinsic template cosine [11]. This implies that combinations with the CMB data will be important for degeneracy breaking in future analyses.

Our aggressive analysis yields noticeably stronger constraints, $f_{NL}^{\text{equil}} = 257^{+300}_{-300}$, $f_{NL}^{\text{ortho}} = -23^{+120}_{-120}$. Most of the improvement here is driven by fixing quadratic bias parameters. In light of the well-known σ_8 tension, we have also varied σ_8 in our aggressive fit, which somewhat loosens the bounds, $f_{NL}^{\text{equil}} = 510^{+320}_{-440}$, $f_{NL}^{\text{ortho}} = -123^{+150}_{-140}$ ($\sigma_8 = 0.728^{+0.033}_{-0.037}$), at 68% CL. Concluding, we emphasize that our aggressive analysis is performed mainly for the purposes of illustration. It demonstrates that PNG constraints can be significantly improved with a better

knowledge of bias parameters, which motivates further work on their calibration with simulations, e.g. along the lines of [73, 74].

We have also repeated our baseline analysis with free n_s and found consistent, albeit somewhat weaker limits $f_{\text{NL}}^{\text{equil}} = 1200^{+630}_{-850}$, $f_{\text{NL}}^{\text{ortho}} = -240^{+210}_{-180}$ (with $n_s = 0.83 \pm 0.08$).

Constraints on early Universe physics — Our main analysis was performed using flat priors on $f_{\text{NL}}^{\text{equil}}, f_{\text{NL}}^{\text{ortho}}$, which map onto non-flat priors of the physical coefficients in the EFT Lagrangian (1). To avoid any potential prior bias, we repeat our MCMC analysis varying directly the relevant parameters $\log_{10} c_s$ and $\tilde{c}_3(c_s^{-2} - 1)$ (following [19]), assuming flat priors $\log_{10} c_s \in (-\infty, 0]$ and $\tilde{c}_3(c_s^{-2} - 1) \in (-\infty, +\infty)$. The corresponding posterior contours are shown in Fig. 2. They yield the bound on the sound speed

$$c_s \geq 0.013 \quad (\tilde{c}_3 \text{ marginalized, 95% CL}) . \quad (15)$$

For DBI inflation [13], where $\tilde{c}_3 = 3(1 - c_s^2)/2$, we find $c_s \geq 0.04$ (95% CL). In general, the parameter \tilde{c}_3 cannot be constrained because of degeneracy with c_s , i.e. \tilde{c}_3 is unbounded in the limit $c_s \rightarrow 1$, where we can only constrain the combination of the two parameters,

$$-3.5 \times 10^4 < \tilde{c}_3(c_s^{-2} - 1) < 1 \times 10^4 \quad (95\% \text{ CL}) . \quad (16)$$

Constraints on c_s do not noticeably improve with the aggressive analysis settings. This is because the $(f_{\text{NL}}^{\text{equil}}, f_{\text{NL}}^{\text{ortho}})$ parameter space excluded by these settings mostly corresponds to the unphysical values $c_s^2 > 1$, $c_s^2 < 0$, and hence does not contribute to our final constraints on this parameter.⁸

Conclusions — In this *Letter* we have presented the first non-CMB constraints on non-local primordial non-Gaussianity, using the BOSS redshift-space clustering data. Our nominal constraints on the orthogonal shape and the inflaton sound speed are competitive with those from the Wilkinson Microwave Anisotropy Probe CMB

data [22]. These constraints will certainly improve with the data from upcoming surveys such as *Euclid* [75] or DESI [76]. Based on their volume w.r.t. BOSS, one may expect a reduction of error bars by a factor of 3. However, the limits from current and future surveys can be improved even further if more bispectrum data is used, e.g. from new triangles with larger wavenumbers, and from the angular dependence captured by higher order harmonics (multipoles) of the redshift-space bispectrum [77]. We leave including this information for future work. In addition, it would be interesting to analyze more complex PNG scenarios, and also include information from the recently measured BOSS galaxy trispectrum [78].

Finally, it is worth noting that the PNG constraints from large-scale structure will further improve with futuristic surveys, such as MegaMapper [79], and 21cm/intensity mapping observations, which will map our Universe at high redshifts where the late-time non-Gaussian clustering background is weak.

Our work thus serves as a proof of principle, and paves the way toward systematic analyses of PNG with upcoming large-scale structure surveys.

Acknowledgments — We are grateful to Alex Barreira, Enrico Pajer, and Fabian Schmidt for valuable comments on the draft. GC acknowledges support from the Institute for Advanced Study. The work of MMI has been supported by NASA through the NASA Hubble Fellowship grant #HST-HF2-51483.001-A awarded by the Space Telescope Science Institute, which is operated by the Association of Universities for Research in Astronomy, Incorporated, under NASA contract NAS5-26555. OHEP thanks the Simons Foundation for support. Parameter estimates presented in this paper have been obtained with the **CLASS-PT** Boltzmann code [51] (see also [80]) interfaced with the **Montepython** MCMC sampler [81, 82]. The triangle plots are generated with the **getdist** package⁹ [83].

⁸ Notice that flat priors on $(f_{\text{NL}}^{\text{equil}}, f_{\text{NL}}^{\text{ortho}})$ do not respect the physical conditions $0 \leq c_s^2 \leq 1$, see Eq. (5) and Ref. [19].

⁹ <https://getdist.readthedocs.io/en/latest/>

- [1] A. D. Linde and V. F. Mukhanov, *Phys. Rev. D* **56**, R535 (1997), arXiv:astro-ph/9610219.
- [2] K. Enqvist and M. S. Sloth, *Nucl. Phys. B* **626**, 395 (2002), arXiv:hep-ph/0109214.
- [3] D. H. Lyth and D. Wands, *Phys. Lett. B* **524**, 5 (2002),

- arXiv:hep-ph/0110002.
- [4] D. H. Lyth, C. Ungarelli, and D. Wands, *Phys. Rev. D* **67**, 023503 (2003), arXiv:astro-ph/0208055.
- [5] G. Dvali, A. Gruzinov, and M. Zaldarriaga, *Phys. Rev. D* **69**, 023505 (2004), arXiv:astro-ph/0303591.
- [6] G. Dvali, A. Gruzinov, and M. Zaldarriaga, *Phys. Rev. D* **69**, 083505 (2004), arXiv:astro-ph/0305548.
- [7] M. Zaldarriaga, *Phys. Rev. D* **69**, 043508 (2004), arXiv:astro-ph/0306006.
- [8] C. T. Byrnes and K.-Y. Choi, *Adv. Astron.* **2010**, 724525 (2010), arXiv:1002.3110 [astro-ph.CO].
- [9] L. Senatore and M. Zaldarriaga, *JHEP* **04**, 024 (2012), arXiv:1009.2093 [hep-th].
- [10] J.-L. Lehners, *Adv. Astron.* **2010**, 903907 (2010), arXiv:1001.3125 [hep-th].
- [11] Y. Akrami *et al.* (Planck), *Astron. Astrophys.* **641**, A9 (2020), arXiv:1905.05697 [astro-ph.CO].
- [12] N. Arkani-Hamed, P. Creminelli, S. Mukohyama, and M. Zaldarriaga, *JCAP* **04**, 001 (2004), arXiv:hep-th/0312100.
- [13] M. Alishahiha, E. Silverstein, and D. Tong, *Phys. Rev. D* **70**, 123505 (2004), arXiv:hep-th/0404084.
- [14] L. Senatore, *Phys. Rev. D* **71**, 043512 (2005), arXiv:astro-ph/0406187.
- [15] X. Chen, M.-x. Huang, S. Kachru, and G. Shiu, *JCAP* **01**, 002 (2007), arXiv:hep-th/0605045.
- [16] P. Creminelli, M. A. Luty, A. Nicolis, and L. Senatore, *JHEP* **12**, 080 (2006), arXiv:hep-th/0606090.
- [17] C. Cheung, P. Creminelli, A. L. Fitzpatrick, J. Kaplan, and L. Senatore, *JHEP* **03**, 014 (2008), arXiv:0709.0293 [hep-th].
- [18] C. Cheung, A. L. Fitzpatrick, J. Kaplan, and L. Senatore, *JCAP* **02**, 021 (2008), arXiv:0709.0295 [hep-th].
- [19] L. Senatore, K. M. Smith, and M. Zaldarriaga, *JCAP* **01**, 028 (2010), arXiv:0905.3746 [astro-ph.CO].
- [20] D. Baumann, D. Green, H. Lee, and R. A. Porto, *Phys. Rev. D* **93**, 023523 (2016), arXiv:1502.07304 [hep-th].
- [21] D. Green and E. Pajer, *JCAP* **09**, 032 (2020), arXiv:2004.09587 [hep-th].
- [22] C. L. Bennett, D. Larson, J. L. Weiland, N. Jarosik, G. Hinshaw, N. Odegard, K. M. Smith, R. S. Hill, B. Gold, M. Halpern, E. Komatsu, M. R. Nolta, L. Page, D. N. Spergel, E. Wollack, J. Dunkley, A. Kogut, M. Limon, S. S. Meyer, G. S. Tucker, and E. L. Wright, "Astrophys. J." **208**, 20 (2013), arXiv:1212.5225 [astro-ph.CO].
- [23] B. Leistedt, H. V. Peiris, and N. Roth, *Phys. Rev. Lett.* **113**, 221301 (2014), arXiv:1405.4315 [astro-ph.CO].
- [24] E. Castorina *et al.*, *JCAP* **09**, 010 (2019), arXiv:1904.08859 [astro-ph.CO].
- [25] E.-M. Mueller *et al.*, (2021), arXiv:2106.13725 [astro-ph.CO].
- [26] M. M. Ivanov, O. H. E. Philcox, T. Nishimichi, M. Simonović, M. Takada, and M. Zaldarriaga, (2021), arXiv:2110.10161 [astro-ph.CO].
- [27] O. H. E. Philcox and M. M. Ivanov, (2021), arXiv:2112.04515 [astro-ph.CO].
- [28] R. Scoccimarro, *Astrophys. J.* **544**, 597 (2000), arXiv:astro-ph/0004086.
- [29] E. Sefusatti, M. Crocce, S. Pueblas, and R. Scoccimarro, *Phys. Rev. D* **74**, 023522 (2006), arXiv:astro-ph/0604505 [astro-ph].
- [30] T. Baldauf, L. Mercolli, M. Mirbabayi, and E. Pajer, *JCAP* **1505**, 007 (2015), arXiv:1406.4135 [astro-ph.CO].
- [31] R. E. Angulo, S. Foreman, M. Schmittfull, and L. Senatore, *JCAP* **1510**, 039 (2015), arXiv:1406.4143 [astro-ph.CO].
- [32] A. Eggemeier, R. Scoccimarro, and R. E. Smith, (2018), arXiv:1812.03208 [astro-ph.CO].
- [33] M. M. Ivanov, M. Simonović, and M. Zaldarriaga, *JCAP* **05**, 042 (2020), arXiv:1909.05277 [astro-ph.CO].
- [34] G. D'Amico, J. Gleyzes, N. Kokron, D. Markovic, L. Senatore, P. Zhang, F. Beutler, and H. Gil-Marín, (2019), arXiv:1909.05271 [astro-ph.CO].
- [35] A. Oddo, E. Sefusatti, C. Porciani, P. Monaco, and A. G. Sánchez, *JCAP* **03**, 056 (2020), arXiv:1908.01774 [astro-ph.CO].
- [36] A. Eggemeier, R. Scoccimarro, R. E. Smith, M. Crocce, A. Pezzotta, and A. G. Sánchez, (2021), arXiv:2102.06902 [astro-ph.CO].
- [37] D. Alkhanishvili, C. Porciani, E. Sefusatti, M. Biagetti, A. Lazanu, A. Oddo, and V. Yankelevich, (2021), arXiv:2107.08054 [astro-ph.CO].
- [38] A. Oddo, F. Rizzo, E. Sefusatti, C. Porciani, and P. Monaco, *JCAP* **11**, 038 (2021), arXiv:2108.03204 [astro-ph.CO].
- [39] S.-F. Chen, Z. Vlah, and M. White, (2021), arXiv:2110.05530 [astro-ph.CO].
- [40] T. Baldauf, M. Garny, P. Taule, and T. Steele, *Phys. Rev. D* **104**, 123551 (2021), arXiv:2110.13930 [astro-ph.CO].
- [41] O. H. E. Philcox, *Phys. Rev. D* **103**, 103504 (2021), arXiv:2012.09389 [astro-ph.CO].
- [42] O. H. E. Philcox, *Phys. Rev. D* **104**, 123529 (2021), arXiv:2107.06287 [astro-ph.CO].
- [43] N. Aghanim *et al.* (Planck), (2018), arXiv:1807.06209 [astro-ph.CO].
- [44] D. Babich, P. Creminelli, and M. Zaldarriaga, *JCAP* **08**, 009 (2004), arXiv:astro-ph/0405356.
- [45] D. Baumann, A. Nicolis, L. Senatore, and M. Zaldarriaga, *JCAP* **1207**, 051 (2012), arXiv:1004.2488 [astro-ph.CO].

- [46] J. J. M. Carrasco, M. P. Hertzberg, and L. Senatore, *JHEP* **09**, 082 (2012), arXiv:1206.2926 [astro-ph.CO].
- [47] V. Desjacques, D. Jeong, and F. Schmidt, *Phys. Rept.* **733**, 1 (2018), arXiv:1611.09787 [astro-ph.CO].
- [48] T. Nishimichi, G. D’Amico, M. M. Ivanov, L. Senatore, M. Simonović, M. Takada, M. Zaldarriaga, and P. Zhang, *Phys. Rev. D* **102**, 123541 (2020), arXiv:2003.08277 [astro-ph.CO].
- [49] E. Sefusatti and E. Komatsu, *Phys. Rev. D* **76**, 083004 (2007), arXiv:0705.0343 [astro-ph].
- [50] E. Sefusatti, *Phys. Rev. D* **80**, 123002 (2009), arXiv:0905.0717 [astro-ph.CO].
- [51] A. Chudaykin, M. M. Ivanov, O. H. E. Philcox, and M. Simonović, *Phys. Rev. D* **102**, 063533 (2020), arXiv:2004.10607 [astro-ph.CO].
- [52] A. Taruya, K. Koyama, and T. Matsubara, *Phys. Rev. D* **78**, 123534 (2008), arXiv:0808.4085 [astro-ph].
- [53] V. Assassi, D. Baumann, E. Pajer, Y. Welling, and D. van der Woude, *JCAP* **11**, 024 (2015), arXiv:1505.06668 [astro-ph.CO].
- [54] A. Moradinezhad Dizgah, M. Biagetti, E. Sefusatti, V. Desjacques, and J. Noreña, *JCAP* **05**, 015 (2021), arXiv:2010.14523 [astro-ph.CO].
- [55] V. Assassi, D. Baumann, and F. Schmidt, *JCAP* **12**, 043 (2015), arXiv:1510.03723 [astro-ph.CO].
- [56] R. Angulo, M. Fasiello, L. Senatore, and Z. Vlah, *JCAP* **1509**, 029 (2015), arXiv:1503.08826 [astro-ph.CO].
- [57] E. Pajer and M. Zaldarriaga, *JCAP* **08**, 037 (2013), arXiv:1301.7182 [astro-ph.CO].
- [58] M. M. Ivanov, M. Simonović, and M. Zaldarriaga, *Phys. Rev. D* **101**, 083504 (2020), arXiv:1912.08208 [astro-ph.CO].
- [59] L. Senatore and M. Zaldarriaga, *JCAP* **1502**, 013 (2015), arXiv:1404.5954 [astro-ph.CO].
- [60] T. Baldauf, M. Mirbabayi, M. Simonović, and M. Zaldarriaga, *Phys. Rev. D* **92**, 043514 (2015), arXiv:1504.04366 [astro-ph.CO].
- [61] D. Blas, M. Garny, M. M. Ivanov, and S. Sibiryakov, *JCAP* **1607**, 052 (2016), arXiv:1512.05807 [astro-ph.CO].
- [62] D. Blas, M. Garny, M. M. Ivanov, and S. Sibiryakov, *JCAP* **1607**, 028 (2016), arXiv:1605.02149 [astro-ph.CO].
- [63] M. M. Ivanov and S. Sibiryakov, *JCAP* **1807**, 053 (2018), arXiv:1804.05080 [astro-ph.CO].
- [64] A. Vasudevan, M. M. Ivanov, S. Sibiryakov, and J. Lesgourgues, *JCAP* **09**, 037 (2019), arXiv:1906.08697 [astro-ph.CO].
- [65] C. Alcock and B. Paczynski, *Nature* **281**, 358 (1979).
- [66] S. Alam *et al.* (BOSS), *Mon. Not. Roy. Astron. Soc.* **470**, 2617 (2017), arXiv:1607.03155 [astro-ph.CO].
- [67] M. M. Ivanov, O. H. E. Philcox, M. Simonović, M. Zaldarriaga, T. Nishimichi, and M. Takada, (2021), arXiv:2110.00006 [astro-ph.CO].
- [68] O. H. E. Philcox, M. M. Ivanov, M. Simonović, and M. Zaldarriaga, *JCAP* **05**, 032 (2020), arXiv:2002.04035 [astro-ph.CO].
- [69] F.-S. Kitaura *et al.*, *Mon. Not. Roy. Astron. Soc.* **456**, 4156 (2016), arXiv:1509.06400 [astro-ph.CO].
- [70] M. Simonović, T. Baldauf, M. Zaldarriaga, J. J. Carrasco, and J. A. Kollmeier, *JCAP* **1804**, 030 (2018), arXiv:1708.08130 [astro-ph.CO].
- [71] R. J. Cooke, M. Pettini, and C. C. Steidel, *Astrophys. J.* **855**, 102 (2018), arXiv:1710.11129 [astro-ph.CO].
- [72] F. Schmidt and M. Kamionkowski, *Phys. Rev. D* **82**, 103002 (2010), arXiv:1008.0638 [astro-ph.CO].
- [73] A. Barreira, T. Lazeyras, and F. Schmidt, (2021), arXiv:2105.02876 [astro-ph.CO].
- [74] T. Lazeyras, A. Barreira, and F. Schmidt, *JCAP* **10**, 063 (2021), arXiv:2106.14713 [astro-ph.CO].
- [75] R. Laureijs *et al.* (EUCLID), (2011), arXiv:1110.3193 [astro-ph.CO].
- [76] A. Aghamousa *et al.* (DESI), (2016), arXiv:1611.00036 [astro-ph.IM].
- [77] R. Scoccimarro, *Phys. Rev. D* **92**, 083532 (2015), arXiv:1506.02729 [astro-ph.CO].
- [78] O. H. E. Philcox, J. Hou, and Z. Slepian, (2021), arXiv:2108.01670 [astro-ph.CO].
- [79] D. J. Schlegel *et al.*, (2019), arXiv:1907.11171 [astro-ph.IM].
- [80] D. Blas, J. Lesgourgues, and T. Tram, *JCAP* **1107**, 034 (2011), arXiv:1104.2933 [astro-ph.CO].
- [81] B. Audren, J. Lesgourgues, K. Benabed, and S. Prunet, *JCAP* **1302**, 001 (2013), arXiv:1210.7183 [astro-ph.CO].
- [82] T. Brinckmann and J. Lesgourgues, *Phys. Dark Univ.* **24**, 100260 (2019), arXiv:1804.07261 [astro-ph.CO].
- [83] A. Lewis, (2019), arXiv:1910.13970 [astro-ph.IM].
- [84] F. Bernardeau, S. Colombi, E. Gaztanaga, and R. Scoccimarro, *Phys. Rept.* **367**, 1 (2002), arXiv:astro-ph/0112551 [astro-ph].
- [85] T. Lazeyras, C. Wagner, T. Baldauf, and F. Schmidt, *JCAP* **1602**, 018 (2016), arXiv:1511.01096 [astro-ph.CO].

Supplemental Material

1. DETAILS OF THE THEORY MODEL

Following the notation of [S51], the Z_2 kernel necessary to derive $P_{12}(\mathbf{k})$ in Eq. (9) is

$$\begin{aligned} Z_2(\mathbf{k}_1, \mathbf{k}_2) = & \frac{b_2}{2} + b_{\mathcal{G}_2} \left(\frac{(\mathbf{k}_1 \cdot \mathbf{k}_2)^2}{k_1^2 k_2^2} - 1 \right) + b_1 F_2(\mathbf{k}_1, \mathbf{k}_2) + f \mu^2 G_2(\mathbf{k}_1, \mathbf{k}_2) \\ & + \frac{f \mu k}{2} \left(\frac{\mu_1}{k_1} (b_1 + f \mu_2^2) + \frac{\mu_2}{k_2} (b_1 + f \mu_1^2) \right), \end{aligned} \quad (\text{S1})$$

where F_2 and G_2 are the SPT kernels [S84]

$$\begin{aligned} F_2(\mathbf{k}_1, \mathbf{k}_2) = & \frac{5}{7} + \frac{2}{7} \frac{(\mathbf{k}_1 \cdot \mathbf{k}_2)^2}{k_1^2 k_2^2} + \frac{1}{2} \frac{\mathbf{k}_1 \cdot \mathbf{k}_2}{k_1 k_2} \left(\frac{k_1}{k_2} + \frac{k_2}{k_1} \right), \\ G_2(\mathbf{k}_1, \mathbf{k}_2) = & \frac{3}{7} + \frac{4}{7} \frac{(\mathbf{k}_1 \cdot \mathbf{k}_2)^2}{k_1^2 k_2^2} + \frac{1}{2} \frac{\mathbf{k}_1 \cdot \mathbf{k}_2}{k_1 k_2} \left(\frac{k_1}{k_2} + \frac{k_2}{k_1} \right), \end{aligned} \quad (\text{S2})$$

and $\mu_i = \hat{\mathbf{k}}_i \cdot \hat{\mathbf{z}}$. Our non-Gaussian model depends on the quadratic bias b_2 and the tidal bias $b_{\mathcal{G}_2}$, which also enter the tree-level bispectrum model. For dark matter halos, these biases have the following approximate dependence on the linear bias b_1 :

$$b_{\mathcal{G}_2} = -\frac{2}{7}(b_1 - 1), \quad b_2 = 0.412 - 2.143b_1 + 0.929b_1^2 + 0.008b_1^3 - \frac{8}{21}(b_1 - 1). \quad (\text{S3})$$

The relationship $b_{\mathcal{G}_2}(b_1)$ follows from the Lagrangian local in matter density model [S47], while the function $b_2(b_1)$ is fit from the halo simulation data [S85]. These relationships, strictly speaking, do not hold for simulated galaxies, but the deviations are not significant given the precision of the current data [S26, S36]. We use the relations (S3) in our aggressive analysis, evaluating them for the best-fit values of b_1 taken from the baseline results.

2. EFFECTS OF PNG ON GALAXY POWER SPECTRA AND BISPECTRA

In this Section we present plots that give some intuition on the source of our f_{NL} constraints. In Fig. S1 we illustrate the effect of variations of the parameters $f_{\text{NL}}^{\text{equil}}, f_{\text{NL}}^{\text{ortho}}, b_2, b_{\mathcal{G}_2}$ on the galaxy bispectrum monopole B . Parameters are varied within the following intervals:

$$f_{\text{NL}}^{\text{equil}} \in [-2000, 2000], \quad f_{\text{NL}}^{\text{ortho}} \in [-1000, 1000], \quad b_2 \in [b_2^{\text{fid}} - 1, b_2^{\text{fid}} + 1], \quad b_{\mathcal{G}_2} \in [b_{\mathcal{G}_2}^{\text{fid}} - 0.5, b_{\mathcal{G}_2}^{\text{fid}} + 0.5], \quad (\text{S4})$$

where $b_2^{\text{fid}}, b_{\mathcal{G}_2}^{\text{fid}}$ are fiducial parameters equal to the best-fit values. We present the residuals $B/B_{\text{fid.}} - 1$ as a function of the triangle index of our bispectrum data vector, where $B_{\text{fid.}}$ is the best-fit bispectrum model for the NGC z3 ($z = 0.61$) data chunk, obtained in the analysis with $f_{\text{NL}}^{\text{equil}} = 0, f_{\text{NL}}^{\text{ortho}} = 0$. Each triangle is labelled by its bin center wavenumbers (k_1, k_2, k_3) , whose magnitudes are constrained to be $k \in [0.015, 0.08] \text{ hMpc}^{-1}$. Indices corresponding to squeezed, equilateral, and flattened configurations are denoted by black, orange, and green dots in the x axis, and a shaded gray contour on the background shows the error bars of the NGC z3 data. We chose the extremal values of the varied parameters in Eq. (S4) such that the resulting residual curve has a 1σ deviation at least for several data points. This suggests that the cumulative χ^2 should be significant, and the corresponding variations should be constrained by the data.

The first important observation is that the parameters of interest have very different shape dependence. $f_{\text{NL}}^{\text{equil}}$ mostly enhances equilateral triangles ($k_1 = k_2 = k_3$); the effect on the squeezed triangles ($k_3 = 0.015 \text{ hMpc}^{-1}, k_1 = k_2, k_1 > k_3$) is somewhat weaker, whilst the flattened triangles ($k_3 = k_2, 2k_2 = k_1 + 0.005 \text{ hMpc}^{-1}$) are affected

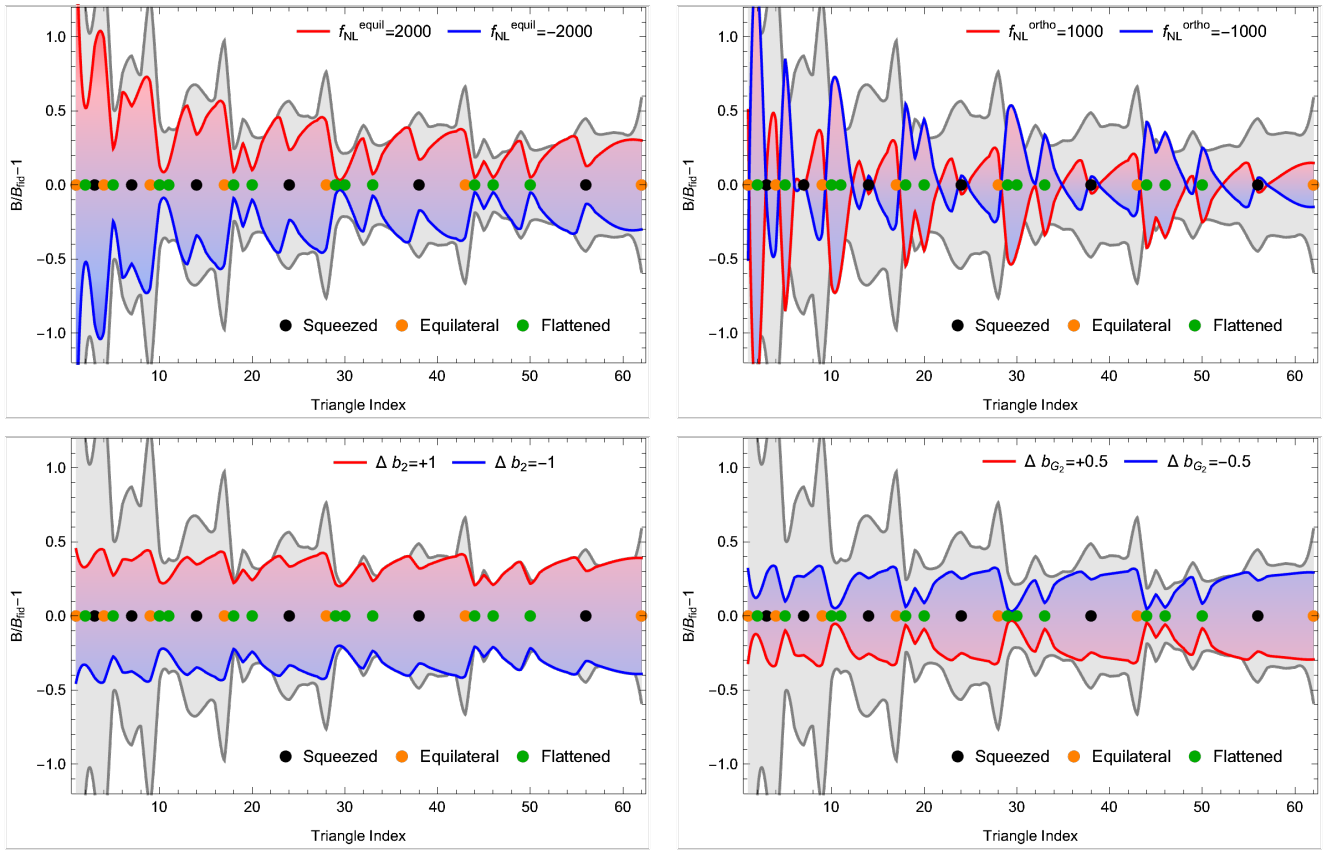


FIG. S1. Residual variations of the galaxy bispectrum monopole w.r.t. variations of $f_{\text{NL}}^{\text{equil}}$ (upper left panel), $f_{\text{NL}}^{\text{ortho}}$ (upper right panel), quadratic bias b_2 (lower left panel), and tidal bias b_{G_2} (lower right panel). Black, orange and green dots denote the squeezed ($k_3 = 0.015 \text{ hMpc}^{-1}$, $k_2 = k_1$), equilateral ($k_1 = k_2 = k_3$), and flattened ($k_2 = k_3$, $2k_2 = k_1 + 0.005 \text{ hMpc}^{-1}$) triangle configurations, respectively. These variations have distinctive shape dependence and therefore can be constrained by the data.

very little. In contrast, $f_{\text{NL}}^{\text{ortho}}$ peaks sharply at the flattened and equilateral triangles. Note that these effects are of the opposite sign, which is a known signature of the orthogonal template. Remarkably, the effect on the squeezed triangles is vanishingly small.

Now let us discuss the quadratic bias parameters, which represent a late-time non-Gaussian contribution. The effect of b_2 is almost uniform for all triangles. In contrast, b_{G_2} noticeably amplifies the squeezed and equilateral triangles, while the flattened triangles are almost unaffected.

All in all, we see that the data should distinguish between the shapes of interest. The qualitative picture of that is as follows. $f_{\text{NL}}^{\text{ortho}}$ is the only shape that sharply peaks at the flattened triangles. In addition, it produces specific “opposite” peaks in the equilateral triangles. Clearly, this pattern cannot be reproduced by any other parameter and hence we do not expect $f_{\text{NL}}^{\text{ortho}}$ to be degenerate with them. The signature of b_2 is also quite unique, as it is the only shape that enhances all triangles in a uniform way. Hence, it should be robustly constrained. The only noticeable degeneracy we expect is between $f_{\text{NL}}^{\text{equil}}$ and b_{G_2} , because both corresponding shapes mostly enhance squeezed and equilateral configurations, while leaving the flattened triangles almost intact. The degeneracy between these gets broken by the relative height of the squeezed and equilateral triangles: b_{G_2} enhances both these triangles uniformly, while $f_{\text{NL}}^{\text{equil}}$ generates some contrast by amplifying more the equilateral configurations.

In Fig. S2 we repeat the same exercise for the galaxy power spectrum monopole P for the wavenumbers relevant for our analysis, $k \in [0.01, 0.2] \text{ hMpc}^{-1}$. We focus on the P_{12} -type matter loop corrections only, because the effects of the

linear PNG bias clearly cannot be constrained without a prior on b_ζ . Looking at Fig. S2, we see that, although power spectrum modulations produced by $f_{\text{NL}}^{\text{equil}} \sim 1000$, $f_{\text{NL}}^{\text{ortho}} \sim 1000$ are nominally larger than the error bars, the signal produced by these shapes is a very smooth function of scale. Thus, the PNG terms are quite degenerate with the Gaussian non-linear corrections, explaining why we cannot get strong constraints on NLPNG from the power spectra alone. For very large $f_{\text{NL}}^{\text{equil}}$, $f_{\text{NL}}^{\text{ortho}}$, however, one can break the degeneracies, i.e. using the non-monotonic behaviour of the $f_{\text{NL}}^{\text{ortho}}$ term on large scales $\lesssim 0.1 h\text{Mpc}^{-1}$. This explains why in the mock simulation data analysis we were able to break degeneracies for very large $f_{\text{NL}}^{\text{ortho}} \sim 1000$. However, the total volume of this simulation was 40 times larger than the actual BOSS survey volume. This demonstrates that the galaxy power spectrum alone does not have enough power to provide any interesting constraints on PNG, though it is still instrumental in breaking parameter degeneracies relevant for the bispectrum, e.g. the notorious degeneracy between b_1 and σ_8 .

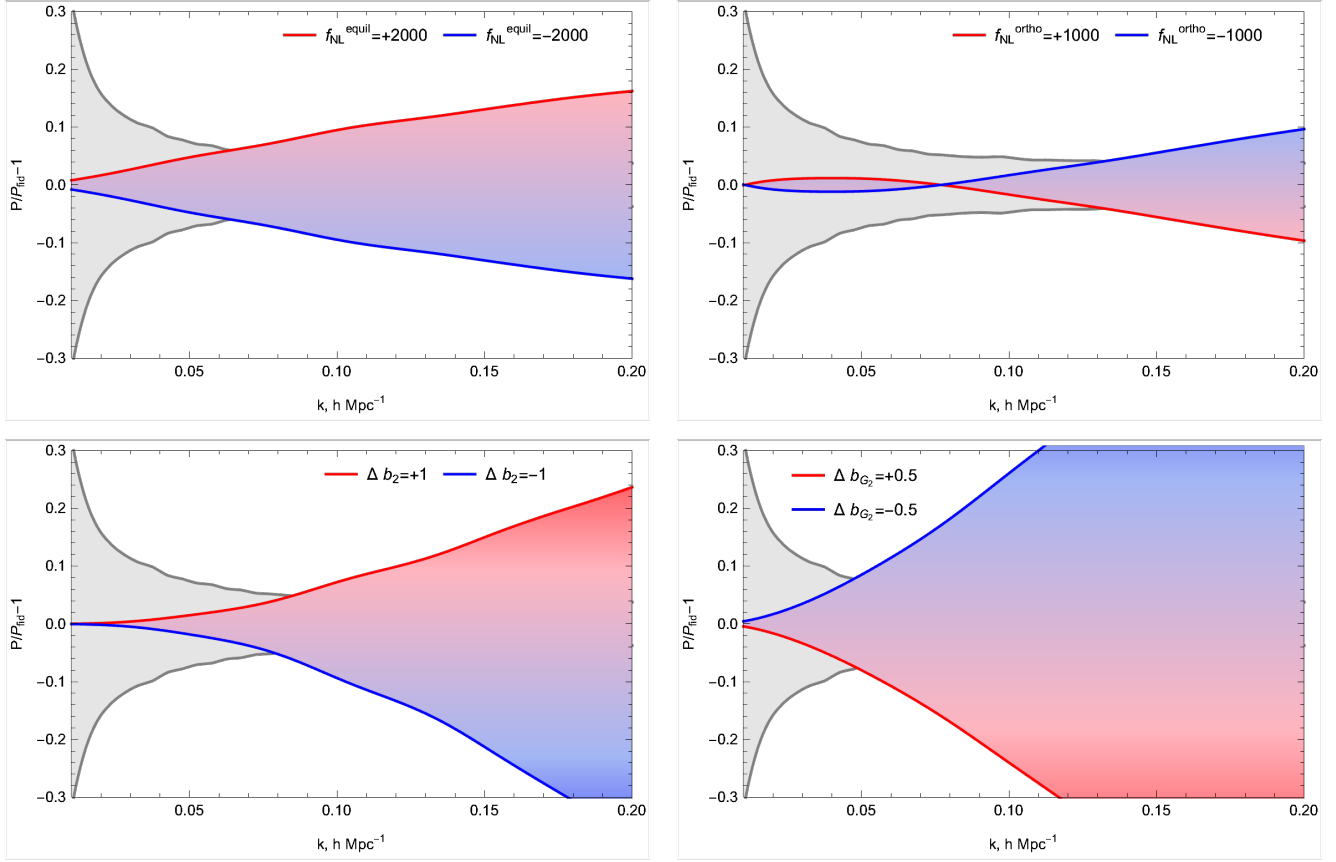


FIG. S2. Residual variations of the galaxy power spectrum monopole P_0 w.r.t. variations of $f_{\text{NL}}^{\text{equil}}$ (upper left panel), $f_{\text{NL}}^{\text{ortho}}$ (upper right panel), quadratic bias b_2 (lower left panel), and tidal bias b_{G_2} (lower right panel).

3. FULL TRIANGLE PLOTS AND CONSTRAINT TABLES

In this Section we present a full triangle plot (Fig. S3) and parameter constraint table (Tab. I) from two PNG analyses of BOSS DR12: (a) with free power spectrum tilt n_s and (b) with a *Planck* prior on n_s . The latter is our baseline choice. We present results for the joint analysis of the full power spectrum, BAO, and bispectrum datasets.

Parameter	BOSS DR12 + free n_s				BOSS DR12, baseline			
	best-fit	mean $\pm \sigma$	95% lower	95% upper	best-fit	mean $\pm \sigma$	95% lower	95% upper
ω_{cdm}	0.1262	$0.1413^{+0.011}_{-0.015}$	0.1159	0.1682	0.1197	$0.1225^{+0.0053}_{-0.0059}$	0.1115	0.1339
h	0.6848	$0.6954^{+0.011}_{-0.013}$	0.6719	0.7195	0.6827	$0.682^{+0.0085}_{-0.0088}$	0.665	0.6992
$\ln(10^{10} A_s)$	2.739	$2.533^{+0.14}_{-0.15}$	2.249	2.826	2.716	$2.728^{+0.1}_{-0.1}$	2.528	2.929
n_s	0.9324	$0.8323^{+0.075}_{-0.074}$	0.6858	0.9801	-	-	-	-
$10^{-2} f_{NL}^{\text{equil}}$	1.82	$12.39^{+6.7}_{-8.6}$	-3.179	28.49	2.278	$9.421^{+5.7}_{-6.5}$	-2.779	21.91
$10^{-2} f_{NL}^{\text{ortho}}$	-0.0628	$-2.484^{+2.1}_{-1.9}$	-6.557	1.484	-0.7874	$-1.732^{+1.8}_{-1.7}$	-5.265	1.756
$b_1^{(1)}$	2.323	$2.404^{+0.14}_{-0.14}$	2.127	2.687	2.408	$2.353^{+0.13}_{-0.14}$	2.078	2.63
$b_2^{(1)}$	0.5561	$0.5731^{+0.84}_{-0.9}$	-1.159	2.295	0.9517	$0.675^{+0.83}_{-0.88}$	-1.012	2.396
$b_{G_2}^{(1)}$	-0.3561	$-0.324^{+0.41}_{-0.46}$	-1.197	0.57	-0.1242	$-0.1568^{+0.41}_{-0.42}$	-0.9911	0.6793
$b_1^{(2)}$	2.502	$2.566^{+0.14}_{-0.15}$	2.282	2.858	2.563	$2.521^{+0.14}_{-0.15}$	2.239	2.809
$b_2^{(2)}$	0.08728	$0.07405^{+0.88}_{-0.91}$	-1.685	1.883	0.4217	$0.1337^{+0.87}_{-0.88}$	-1.617	1.86
$b_{G_2}^{(2)}$	-0.2795	$-0.1499^{+0.43}_{-0.49}$	-1.079	0.8198	-0.1956	$-0.06784^{+0.45}_{-0.47}$	-0.9817	0.8616
$b_1^{(3)}$	2.198	$2.299^{+0.12}_{-0.14}$	2.041	2.561	2.26	$2.242^{+0.12}_{-0.13}$	1.99	2.499
$b_2^{(3)}$	-0.03962	$-0.05736^{+0.77}_{-0.78}$	-1.631	1.503	0.2868	$0.08216^{+0.75}_{-0.77}$	-1.428	1.617
$b_{G_2}^{(3)}$	-0.4604	$-0.4348^{+0.3}_{-0.33}$	-1.087	0.2549	-0.3913	$-0.3014^{+0.35}_{-0.37}$	-1.022	0.4259
$b_1^{(4)}$	2.223	$2.348^{+0.13}_{-0.15}$	2.073	2.636	2.317	$2.293^{+0.13}_{-0.14}$	2.025	2.564
$b_2^{(4)}$	-0.04403	$-0.2223^{+0.83}_{-0.84}$	-1.913	1.461	0.01938	$-0.1926^{+0.77}_{-0.83}$	-1.79	1.433
$b_{G_2}^{(4)}$	-0.1569	$-0.1981^{+0.37}_{-0.37}$	-0.9765	0.5782	-0.3865	$-0.2292^{+0.39}_{-0.41}$	-1.028	0.5808
Ω_m	0.3183	$0.3394^{+0.018}_{-0.02}$	0.3022	0.3778	0.3062	$0.3129^{+0.0096}_{-0.01}$	0.2932	0.333
H_0	68.48	$69.54^{+1.1}_{-1.3}$	67.19	71.95	69.44	$69.57^{+1.1}_{-1.3}$	67.19	72.03
σ_8	0.7124	$0.663^{+0.038}_{-0.042}$	0.5841	0.7452	0.689	$0.7039^{+0.034}_{-0.038}$	0.6335	0.7753

TABLE I. Full parameter constraints from the analysis of full BOSS DR12 data including the bispectrum, combined with a BBN prior on the ω_b (both columns), and an additional Planck prior on n_s (right columns). We present the best-fit values, the mean, 68%, and 95% confidence level results in each case, and show the derived parameters in the bottom rows. The superscripts on bias parameters indicate the sample, in the order NGC z3, SGC z3, NGC z1, SGC z1. The associated two-dimensional posteriors are shown in Fig. S3.

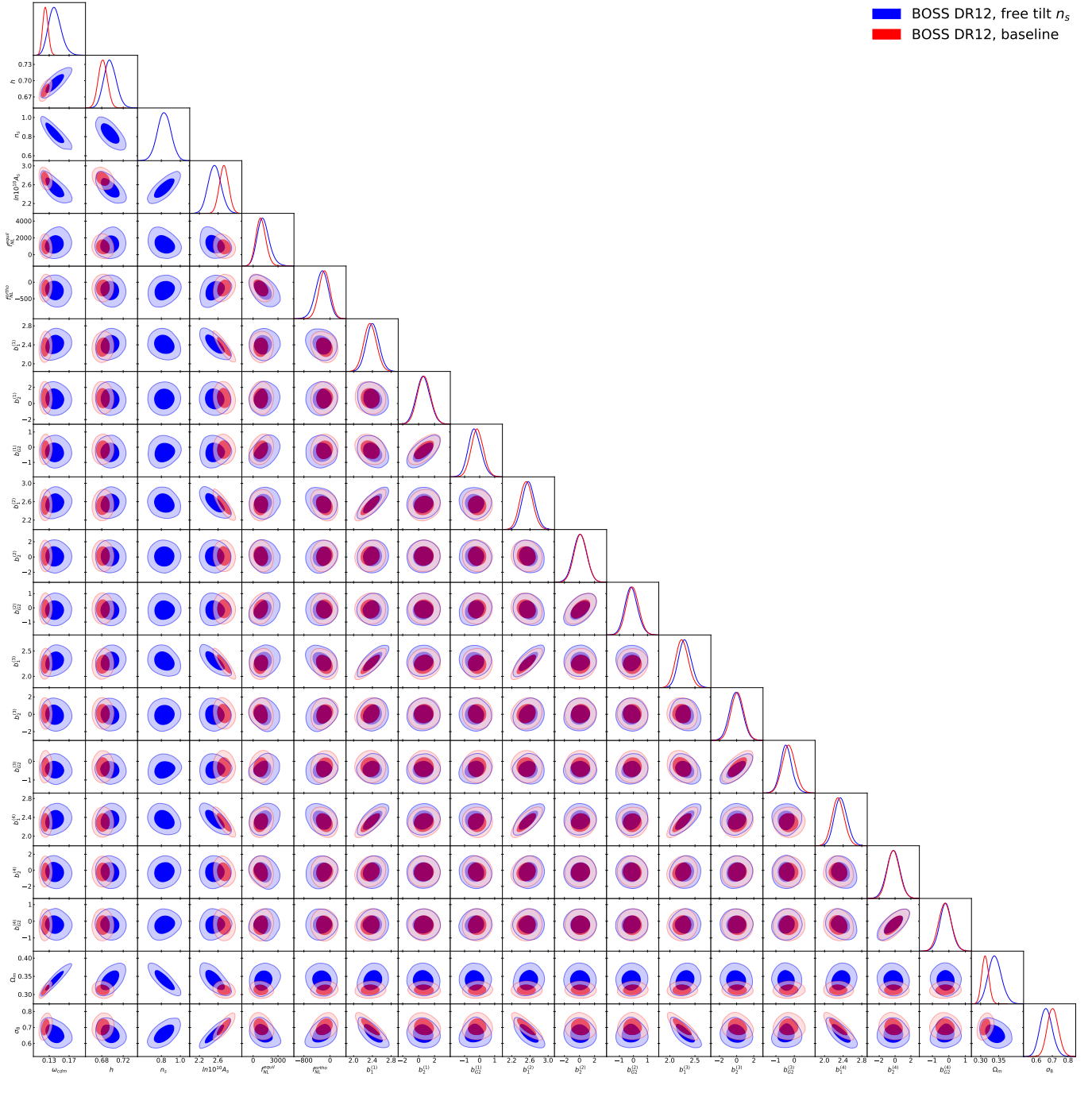


FIG. S3. Full posterior plot of the cosmological and nuisance parameter posteriors measured from the BOSS DR12 data (with a BBN prior on the ω_b), with the free power spectrum tilt n_s (blue contours) and with n_s fixed to the *Planck* prior (red contours, baseline choice). The corresponding parameter constraints are given in Tab. I.